Journal of Computational Physics 229 (2010) 8180–8198

Contents lists available at ScienceDirect

Journal of Computational Physics

journal homepage: www.elsevier.com/locate/jcp

Simulation of coherent structures in nonlinear Schrödinger-type equations

I. Alonso-Mallo [a,1], A. Durán [b,*], N. Reguera [c]

[a] Departamento de Matemática Aplicada, Facultad de Ciencias, Universidad de Valladolid, C/Dr. Mergelina s/n, 47011 Valladolid, Spain
[b] Departamento de Matemática Aplicada, E.T.S.I. Telecomunicación, Campus Miguel Delibes, Universidad de Valladolid, Paseo de Belen 15, 47011 Valladolid, Spain
[c] Departamento de Matemáticas y Computación, Escuela Politécnica Superior, Universidad de Burgos, Avda. de Cantabria s/n, 09006 Burgos, Spain

ARTICLE INFO

Article history:
Received 10 February 2010
Received in revised form 14 July 2010
Accepted 19 July 2010
Available online 29 July 2010

Keywords:
Nonlinear Schrödinger-type equations
Ground states
Conserved quantities
Finite element methods
Conservative integration

ABSTRACT

This paper presents some numerical methods to simulate the evolution of coherent structures with small fluctuations, that appear as typical solutions of a class of nonintegrable nonlinear Schrödinger equations. The construction of the methods is particularly focused on two points: on one hand, the generation of the ground state profiles, to be used in the initial data of the simulations, combines a suitable spatial discretization with the resolution of a discrete variational problem. On the other hand, the approximation to leading parameters of these structures is controlled by the time integration. We compare different methods when simulating the evolution of initial ground state profiles and some initial data perturbed from them.

1. Introduction

The purpose of this work is the construction of numerical methods to simulate the dynamics of ground state solutions of nonlinear Schrödinger-type (NLS) equations with homogeneous Dirichlet boundary conditions. The main points of the study are the approximation to the initial ground state profile, the spatial discretization and the simulation of the parameters that govern the angular velocity and the phase of the ground state evolution. The numerical experiments include simulations of these ground states and of different perturbations.

The physical motivation of the paper is in the study of nonsingular wave turbulence in plasma and fluid models, governed by different models [31,43–45]. Among them, those governed by focusing, free of wave collapse, nonlinear Schrödinger equations have a relevant role [16,25,32]. They include both integrable and not integrable cases.

All these physical phenomena point out the interest in studying the generation and persistence of coherent structures in the models. From a numerical point of view, the simulation of the dynamics of these solutions contains some points of interest, from which we emphasize three of them. The first one is the generation of an initial profile of the structure, which is typically unknown and is sometimes associated to minimizing problems (see e.g. [18,13] and references therein). The second one is the use of a suitable discretization in space, which takes into account the localized character of the structure and helps to obtain the initial profile in a simpler way [6]. Finally, the evolution of these structures are sometimes governed by parameters which, at the same time, are related to some aspects of the dynamics, such as conserved quantities or symmetries. A correct simulation of these parameters are in some sense associated to the choice of the time integration [26].

A good performance of the numerical method about these points may be also important in the study of the stability of these structures, since many models predict that solutions trend to evolve towards coherent structures in a sea of small

* Corresponding author.
E-mail addresses: isaias@mac.uva.es (I. Alonso-Mallo), angel@mac.uva.es (A. Durán), nreguera@ubu.es (N. Reguera).
[1] Tel.: +34 983423769; fax: +34 983423013.

0021-9991/$ - see front matter © 2010 Elsevier Inc. All rights reserved.
doi:10.1016/j.jcp.2010.07.018

turbulence or radiation [25,56,57]. An additional point of interest is then to study if the improvements of the methods, obtained when integrating coherent structures, are retained when simulating perturbations or more general solutions. These experiments make up a good test for the methods, since they may require a longer time of simulation and usually involve perturbed structures that must be approximated in a proper way.

The present paper analyzes these problems for the case of NLS equations with homogeneous Dirichlet boundary conditions. Many works in the literature deal with the numerical treatment of NLS models, for the initial value problem, the periodic case or with different boundary conditions on a bounded domain, and including several dimensions. The spatial discretization is carried out with different techniques, such as finite differences [23,65,61,62,1,34,53,58], finite element methods [41,5,7,76], Fourier spectral methods and generalizations [68,71,10,11], Hermite expansions of the numerical solution [12] or methods based on the eigenfunctions of the operator $-d^2/dx^2$ [31,43–45]. On the other hand, the methods of computation of ground states include, among others, Newton's methods ([15] and references therein), Petviashvili's methods and generalizations [55,48,49,54], spectral renormalization methods [2], the use of a normalized gradient flow [9], Runge–Kutta schemes [29] and direct minimization techniques of the energy functional [13,18]. Finally, the treatment of the time integration covers finite-difference techniques (including symplectic methods, specific energy-preserving schemes, integrable discretizations or linearly implicit methods, e.g. [41,61,62,65,23,1,4,59,58,69,75,34,53]), time-splitting techniques [71,10–12] and explicit, time-staggered schemes [22].

The paper is structured as follows. We shall begin, in Section 2, with a description of the NLS model considered. The properties we emphasize are the general nonintegrable character of the problem, its conserved quantities and the way to obtain the ground states. Section 3 is devoted to the description of the numerical techniques to approximate the problem. The spatial discretization is based on cubic finite elements, takes advantage of the localized character of the ground states and is used to generate the initial ground state profile in a suitable form. On the other hand, the choice of the time integrator takes into account the preservation, through the numerical evolution, of discretized versions of the invariant quantities of the problem. Finally, some numerical experiments are discussed in Section 4. Here we take a cubic nonlinearity as a model. With the choice of this relevant case we also wish to show that the discretizations previously described add some computational advantages to the implementation of this problem (which will be explained at the beginning of the section). But we emphasize that other nonlinearities can be treated. The numerical results are divided into two groups. The first one concerns the simulation of ground states, from approximated initial profiles, obtained by our technique. They allow to establish a first selection of the methods, specially as far as the time integrator is concerned. The second group of experiments studies the behaviour of the numerical schemes when simulating perturbations of ground states, with a long time of integration. Its goal is analyzing if the methods with a better performance when approximating ground states retain this good behaviour in perturbed solutions. A particular attention is paid to the simulation of the parameters of new structures that emerge from the perturbations.

2. Description of the model

We consider nonlinear Schrödinger equations on a bounded interval $[0,L]$ with homogeneous Dirichlet boundary conditions of the form:

$$\left.\begin{aligned} &i\Psi_t + \Psi_{xx} + f(|\Psi|^2)\Psi = 0, \quad t > 0, \;\; 0 \leqslant x \leqslant L, \\ &\Psi(0,t) = \Psi(L,t) = 0, \quad t > 0, \\ &\Psi(x,0) = \Phi(x), \quad 0 \leqslant x \leqslant L, \end{aligned}\right\} \tag{1}$$

where $\Psi = \Psi(x,t)$ is complex and f is a real function which represents the nonlinear term. The equation in (1), either one or multi-dimensional, appears in many physical applications, such as waves in plasmas and propagation in optical fibers ([66,16,3,67,38,40,39,47], among others). The particular case given by $f(x) = x$ corresponds to the classical cubic Schrödinger equation.

The nonlinearity f and the boundary conditions affect, among other properties, the integrable character of the equation. Integrability is assured for the cubic case and the initial value problem or the periodic problem [74,73,50]. For other boundary conditions, see e.g. [14,33] and references therein. In particular, for the Dirichlet problem and the focusing cubic case, under certain conditions, the solution of (1) can be written in terms of the solution of a 2×2 matrix Riemann–Hilbert problem [33]. For other cases of nonlinear terms and boundary conditions, integrability is, to our knowledge, unknown, while it is unknown for other cases of nonlinear terms or boundary conditions. In particular, we will assume that f is focusing, i.e. it satisfies $f(x) > 0, f'(x) > 0$ for $x > 0$, in such a way that (1) is nonintegrable, free of wave collapse and with solitary wave solutions. Under these assumptions, the Hamiltonian energy

$$H(\Psi) = \frac{1}{2}\int_0^L |\Psi_x|^2 dx - \frac{1}{2}\int_0^L F(|\Psi|^2) dx, \tag{2}$$

where $F(a) = \int_0^a f(y)dy$ and the particle number

$$N(\Psi) = \frac{1}{2}\int_0^L |\Psi|^2 dx \tag{3}$$

are invariant quantities. The Hamiltonian structure of (1) is determined by H. Unlike the initial value problem or the periodic case, the Dirichlet problem does not admit the spatial translations as a symmetry group. This implies the associated quantity (sometimes called momentum)

$$\mathrm{Im}\int_0^L \Psi\Psi_x\,dx$$

is not preserved by the solutions of (1).

Some works in the literature (e. g. [64,25,56,57,31]) suggest a soliton turbulence behaviour of solutions of the NLS model for long times with different boundary conditions. The field Ψ tends to form persistent coherent structures in a sea of small turbulent fluctuations. In the focusing case, this coherent structure would have the form of a spatial localized ground state [45,43,44]. Then a coherent structure would take the form

$$\Psi(x,t) = \Phi(x)e^{-i\lambda t}, \tag{4}$$

where Φ is the solution of the problem

$$\left.\begin{aligned} &\Phi_{xx} + f(|\Phi|^2)\Phi + \lambda\Phi = 0, \quad 0 \leqslant x \leqslant L,\\ &\Phi(0) = \Phi(L) = 0. \end{aligned}\right\} \tag{5}$$

In terms of the quantities (2) and (3), we can rewrite (5) as

$$\delta H(\Phi) + \lambda\delta N(\Phi) = 0, \tag{6}$$

where δ denotes the variational derivative. In fact, it is known that the functions $\Phi(x)$ are minimizers of the Hamiltonian subject to a given value of particle number [72,35,45]. This means that $\Phi(x)$ is the solution of the variational problem

$$H(\varphi) \to \min \quad \text{subject to } N(\varphi) = N_0. \tag{7}$$

Then (6) is the necessary condition of critical point, with λ as the Lagrange multiplier. Notice that the ground state (4) consists of a profile Φ, solution of (5), which rotates with angular velocity $-\lambda$. Due to the symmetry group of (1) of gauge transformations, each solution Φ of (5) defines an orbit of solutions

$$\Phi_\theta(x) = \Phi(x)e^{-i\theta}, \quad \theta \in \mathbb{R}.$$

From any of these profiles as initial data, the corresponding ground state can be obtained by applying the one-parameter group of rotations, with parameter $\lambda t, t \in \mathbb{R}$. Then the functions

$$\Psi(x,t,\theta,\lambda) = \Phi_\theta(x)e^{-i\lambda t} = \Phi(x)e^{-i(\lambda t+\theta)}, \tag{8}$$

make up a two-parameter family of ground states which are solutions of the problem (1). The parameter θ represents a phase.

3. Description of the numerical methods

Our search for improvements in the performance of numerical integrators to simulate ground states of (1), or perturbations of ground states, is focused, as mentioned above, on three points: the spatial discretization, the generation of the initial profiles and the simulation of the ground state parameters.

The numerical approximation is obtained by using the method of lines. That is, we consider separately the spatial discretization and the time integration.

3.1. Spatial discretization. Cubic finite elements

We first introduce the spatial discretization. There are several possibilities, which include finite differences, spectral or finite element methods (see the references in the Introduction). It is important for us to keep the geometric properties of the solutions of (1) [20] and a natural discretization of the invariants (2) and (3). To this end, we take $\mathcal{V} = H_0^1(0,L) \subset X = L^2(0,L)$($\mathcal{V}$ is the Sobolev space of squared integrable functions in $(0,L)$, with homogeneous Dirichlet boundary conditions, whose weak derivative is also squared integrable) and we consider a weak version of (1): finding $u(t) \in \mathcal{V}$ such that

$$\left.\begin{aligned} &\left\langle \tfrac{du}{dt}, w\right\rangle + i\langle \partial_x u, \partial_x w\rangle = i\langle f(|u|^2)u, w\rangle \quad \forall w \in \mathcal{V},\ \ t \geqslant 0\\ &u(0) = u_0. \end{aligned}\right\} \tag{9}$$

Then we take a parameter h of the spatial discretization and a family of finite dimensional spaces $\mathcal{V}_h \subset H_0^1(0,L)$ that approximate $\mathcal{V}$ and are based on the finite element method. Given $u_{0,h} \in \mathcal{V}_h$, an approximation to the initial condition u_0, we obtain a semidiscrete weak formulation of (1): finding $u_h(t) \in \mathcal{V}_h$, such that,

$$\left.\begin{array}{l}\left\langle \frac{du_h}{dt}, w_h \right\rangle + i\langle \partial_x u_h, \partial_x w_h\rangle = i\langle f(|u_h|^2)u_h, w_h\rangle \quad \forall w_h \in \mathcal{V}_h, \ \ t \geqslant 0,\\ u_h(0) = u_{0,h}.\end{array}\right\} \tag{10}$$

In this paper, we define $\mathcal{V}_h$ as the space of Hermite piecewise cubic polynomial functions, which are continuous and with continuous derivative, and satisfying homogeneous Dirichlet boundary conditions. This choice was considered and justified in [6]. If we take $h = L/J > 0$ with $J \in \mathbb{N}$, $x_j = jh$ for $0 \leqslant j \leqslant J$, let $\{\sigma_j\}_{j=1}^{J-1} \bigcup \{\widetilde{\sigma}_j\}_{j=0}^{J}$ be the shape functions that define a basis of $\mathcal{V}_h$. Then, an element $\Psi_h \in \mathcal{V}_h$ can be written as

$$\Psi_h(x) = \sum_{j=1}^{J-1} \Psi_j \sigma_j(x) + \sum_{j=0}^{J} \widetilde{\Psi}_j \widetilde{\sigma}_j(x), \tag{11}$$

where, due to the choice of the shape functions, we have $\Psi_j = \Psi_h(x_j)$, $1 \leqslant j \leqslant J-1$ and $\widetilde{\Psi}_j = \partial_x \Psi_h(x_j)$, $0 \leqslant j \leqslant J$.

According to this, we look for an approximation $u_h(x,t) \in \mathcal{V}_h$, to the solution $u(x,t)$ of (1), of the form

$$u_h(x,t) = \sum_{j=1}^{J-1} u_j(t)\sigma_j(x) + \sum_{j=0}^{J} \widetilde{u}_j(t)\widetilde{\sigma}_j(x), \tag{12}$$

where $u_j(t)$, $1 \leqslant j \leqslant J-1$ and $\widetilde{u}_j(t)$, $0 \leqslant j \leqslant J$ are respectively the corresponding approximations to $u(x_j,t)$, $1 \leqslant j \leqslant J-1$ and $\partial_x u(x_j,t)$, $0 \leqslant j \leqslant J$. The application of (12) into (10) leads to a system of ordinary differential equations

$$R_h \frac{dU}{dt} = M_h U + \phi(U), \tag{13}$$

where

$$U = [\tilde{u}_0, u_1, \tilde{u}_1, u_2, \tilde{u}_2, \ldots, u_{J-1}, \tilde{u}_{J-1}, \tilde{u}_J]^T,$$

R_h and M_h are symmetric matrices and $\phi(\cdot)$ represents the nonlinear term.

With this construction of the semidiscrete version, the canonical Hamiltonian structure is conserved and the discrete Hamiltonian of an element $\Psi_h \in \mathcal{V}_h$ is given by

$$H(\Psi_h) = \frac{1}{2}\int_0^L |(\Psi_h)_x|^2 dx - \frac{1}{2}\int_0^L F(|(\Psi_h)|^2) dx,$$

that is, the discrete Hamiltonian is the exact Hamiltonian of the piecewise cubic polynomial Ψ_h.

Similarly, the discrete particle number of an element $\Psi_h \in \mathcal{V}_h$ is given by

$$N(\Psi_h) = \frac{1}{2}\int_0^L |\Psi_h|^2 \, dx$$

and it is also a conserved quantity of the problem (10).

Some other alternatives in the spatial discretization are possible. It is also of interest, in our opinion, to emphasize the fact that the spatial discretization adapts to the localized character of the ground states. Since the basis of $\mathcal{V}_h$ is local, the representation (12) is particularly suitable to identify the components of the solution, specially in ground state perturbations. This is useful if, for instance, one is interested in filtering the fluctuations. A local basis would allow to identify those coefficients affected by the turbulence more clearly.

3.2. Generation of initial profiles

The computation of ground states of nonlinear Schrödinger-type equations makes use of different approaches in the literature ([30,63,24,9] among others). They also include Newton's schemes [15], fixed point iterations with stabilizing factors or renormalization methods [55,2,48,49,54], techniques based on the direct minimization of the energy functional, by using finite element methods [13] or a spectral representation of the solution into Hermite functions [18] combined, in both cases, with Newton-like methods for the corresponding nonlinear minimization problem. All these works concern the computation of ground state solutions of the corresponding initial value problem and include several dimensions.

In our case, a direct minimization of the energy functional is also considered, while the spatial discretization determines the technique of computation of the ground states of (1). We also use, as in [13], finite element methods, but with a different basis functions. We consider a discrete version of (7) and search for solutions $\Phi_h \in \mathcal{V}_h$ (that is, Hermite piecewise cubic polynomial functions) of the discrete variational problem

$$H(\Psi_h) \to \min \quad \text{subject to} \quad \psi_h \in \mathcal{V}_h, \ N(\Psi_h) = N_0, \tag{14}$$

where N_0 is a constant value.

In practice, (14) can be numerically solved with a real, standard optimization algorithm. To this end, we consider formula (11) and write Ψ_j, $\widetilde{\Psi}_j$ in the form $\Psi_j = v_j + iw_j$, $j = 1,\ldots,J-1$, $\widetilde{\Psi}_j = \tilde{v}_j + i\tilde{w}_j$, $j = 0,\ldots,J$. Then

$$H(\Psi_h) = \widetilde{H}(v_1, w_1, \ldots, v_{J-1}, w_{J-1}, \tilde{v}_0, \tilde{w}_0, \ldots, \tilde{v}_J, \tilde{w}_J) = \widetilde{H}(v, w, \tilde{v}, \tilde{w}) \tag{15}$$

and similarly,

$$N(\Psi_h) = \widetilde{N}(v_1, w_1, \ldots, v_{J-1}, w_{J-1}, \tilde{v}_0, \tilde{w}_0, \ldots, \tilde{v}_J, \tilde{w}_J) = \widetilde{N}(v, w, \tilde{v}, \tilde{w}),$$

where $\widetilde{H}$, $\widetilde{N}$ are the expressions of N and H in terms of the nodal values of Ψ_h. Thus, (14) can be rewritten as

$$\widetilde{H}(v, w, \tilde{v}, \tilde{w}) \to \min \quad \text{subject to } \widetilde{N}(v, w, \tilde{v}, \tilde{w}) = N_0, \tag{16}$$

which can be solved by means of standard algorithms. Notice that, in order to obtain sufficiently accurate numerical profiles, (16) will usually involve a large number of variables. On the other hand, the parameter λ, associated to the numerical profile, can also be estimated, in an initial stage, by using the corresponding Lagrange multiplier.

3.3. Time discretization

We now analyze the time integration. Since the ground states are determined by the profile Φ and the angular velocity λ, a qualitatively good simulation depends on the accuracy in the approximation to these elements. In the previous subsection, the way selected to generate the initial profile has been explained. On the other hand, for a correct simulation of λ, the choice of the time integrator plays a relevant role.

The preservation of discrete versions of invariant quantities of the problem through the numerical integration is very present in the literature on time integration of differential equations as a desirable property for a method to be competitive ([36,60,52,19] and references therein). Some recent results (see e.g. [28]) show that a better simulation of the parameters of soliton solutions of the initial value problem for some nonlinear Schrödinger equations is related to the preservation, through the numerical integration, of some invariants of the problem. This is obtained when studying the time propagation of the approximation errors in time semidiscrete schemes. Explicitly, the time integration generates some secular components of the error, associated to parameters. Those methods that preserve discretized versions of some invariants of the problem manage to vanish these secular terms. See [20] for an analysis of fully discrete methods.

According to these arguments, we think that, in our case, the preservation of the invariants H and N by the numerical solution must be, among others, a property to be taken into account when choosing the time integrator. Our idea consists of choosing a first numerical method, paying attention to other requirements of the problem. Then this method is modified to preserve the corresponding discrete versions of the invariants.

We first consider the simply diagonally implicit Runge–Kutta (SDIRK) method of order three and tableau

$$\begin{array}{c|cc} c & \mathcal{A} \\ & b^T \end{array} = \begin{array}{c|ccc} \frac{3+\sqrt{3}}{6} & \frac{3+\sqrt{3}}{6} & 0 \\ \frac{3-\sqrt{3}}{6} & \frac{-\sqrt{3}}{3} & \frac{3+\sqrt{3}}{6} \\ & \frac{1}{2} & \frac{1}{2} \end{array} \tag{17}$$

This method is selected for various reasons. Notice first that, after the spatial discretization, the system (13) is oscillatory, so implicitness is necessary. Since the matrix $\mathcal{A}$ is lower triangular and all the elements in the diagonal are identical, considerable gain in computational cost is achieved when the implicit systems for the intermediate stages are solved at each step. On the other hand, (17) will be modified below, in order to preserve (2) and (3). Notice then that the complex left half-plane is included in the absolute stability region of (17). This property of A-stability (obtained by forcing the conservation of N and H) implies the inclusion of arbitrarily large pure imaginary eigenvalues of the linear semidiscrete operator in (10) into the stability region.

Other possibilities can substitute the method (17) [46]. Among them, time-splitting algorithms have been recently used for the Schrödinger and cubic NLS equations. In the second case, the approximation of the initial value problem by methods of order two and four is treated in [10,12]. The convergence of a Strang splitting method is analyzed in [51,17].

Other three time integrators, modified from (17) to include the preservation of the quantities, are considered. This preservation can be done by projecting the numerical approximation onto the manifold levels, defined by the functional H and N. We make a brief description of this procedure in our case, see e.g. [36] for details. Let H_0, N_0 be constants and consider the following three submanifolds of $\mathcal{V}$:

$$\mathcal{M}_1 = \{\Psi \in H_0^1 : H(\Psi) = H_0\},$$
$$\mathcal{M}_2 = \{\Psi \in H_0^1 : N(\Psi) = N_0\},$$
$$\mathcal{M}_3 = \{\Psi \in H_0^1 : H(\Psi) = H_0,\ N(\Psi) = N_0\} = \mathcal{M}_1 \cap \mathcal{M}_2.$$

Taking $H_0 = H(u_0)$ and $N_0 = N(u_0)$, the exact solution of (9) satisfies $u(t) \in \mathcal{M}_i, i = 1, 2, 3$. The idea is to use a projection on these submanifolds in order to assure that the numerical approximation conserves one or both invariant quantities. Suppose that, for some $i = 1, 2, 3$, $U_n \in \mathcal{M}_{h,i} = \mathcal{M}_i \cap \mathcal{V}_h$, where U_n is the numerical approximation to $u(t_n)$ for some time discrete value $t_n > 0$. The following approximation U_{n+1} to $u(t_{n+1})$, being $t_{n+1} = t_n + \Delta t$, is carried out in the following way:

(1) Compute $\widetilde{U}_{n+1}$ by means of the SDIRK method (17).
(2) Project the value $\widetilde{U}_{n+1}$ onto $\mathcal{M}_{h,i}$ to obtain $U_{n+1} \in \mathcal{M}_{h,i}$.

The computation of U_{n+1} involves the resolution of a constrained minimization problem. For example, if we want to conserve the Hamiltonian (the case of the particle number is similar), we have to solve

$$\|\widetilde{U}_{n+1} - U_{n+1}\| \to \min \quad \text{subject to } g(U_{n+1}) = 0, \tag{18}$$

where $g(U) = \widetilde{H}(U) - H_0$, $\widetilde{H}(U)$ is given in (15).

As far as the resolution of (18) is concerned, we consider the Lagrangian function

$$L(U_{n+1}, \mu) = \|\widetilde{U}_{n+1} - U_{n+1}\|^2/2 - g^T(U_{n+1})\mu.$$

From the necessary condition $\partial L/\partial U_{n+1} = 0$, we obtain the system

$$\begin{aligned} U_{n+1} &= \widetilde{U}_{n+1} + g'(U_{n+1})^T\mu, \\ 0 &= g(U_{n+1}), \end{aligned} \tag{19}$$

which can be efficiently solved for μ by means of an iterative procedure. Notice that the computational cost of this one-dimensional system is negligible, compared to that of the SDIRK method. Furthermore, due to the third order of the method, the approximation $\widetilde{U}_{n+1}$, provided by (17), is a good initial value for the iteration. On the other hand, the case of a projection onto $\mathcal{M}_3$ can be described in a similar way, with the difference that in that case $g(U) = (\widetilde{H}(U) - H_0, \widetilde{N}(U) - N_0)$ and, consequently, μ will have two components.

The inclusion of the projection technique in (17), to assure the preservation of the invariants, is simple to implement and computationally cheap, since the iteration for (19) usually converges fast. For an analysis about the convergence of the projection technique, see e.g. [37,36] and references therein. In this context, the projection technique is also used in the approximation to the cubic NLS with symmetric exponential integrators [21]. On the other hand, the splitting methods studied in [51,17,70] preserve the corresponding particle number.

4. Numerical experiments

In this section we show some numerical experiments obtained with the methods previously explained. All of them are carried out for Eq. (1) with $f(x) = x$, that is, we consider a cubic nonlinear term. Apart from its own interest, another reason for this choice is that, in our case, after the spatial discretization, the exact formula for the nonlinear term in (13) can be obtained, with some effort, by using symbolic calculus. Other nonlinearities can be implemented, and they would require the use of numerical quadrature.

The experiments are divided into two groups. The first subsection will focus on the simulation of ground states, while the second one will deal with experiments of perturbations of the initial profiles. In both cases, some comparisons between the numerical methods will be carried out, in order to suggest the most competitive one in each case.

4.1. Simulation of ground states

The classical analysis in the numerical integration of differential equations, based on the construction of highly accurate numerical methods, has to be complemented with the study of other properties when the time of simulation is longer. They are related to the fact that, for long times, the numerical integration should take into account the correct simulation of some geometric aspects of the system under study. This is part of the ideas behind the so-called geometric integration (see e.g. [36]). The application of these ideas to our case implies that a good performance of the numerical method with respect to the two elements that determine the ground state (the profile Φ and the parameter λ) should generate a more proper simulation, in a qualitative sense, for long times. An additional point is the connection in the computation of Φ and λ, due to (6).

Then, our first objective is to obtain ground state profiles which will be used as initial conditions in our numerical experiments. To this end, we solve problems (16) with the numerical routine E04UCF of NAG Fortran 77 Library, Mark 19. This routine is designed to minimize an arbitrary smooth function subject to constraints using a sequential quadratic programming algorithm. More details on the routine may be obtained in [42]. All the profiles used in this paper were computed with this NAG routine until the convergence was reached. The accuracy of the ground states profiles is also guaranteed by our next numerical results.

We first consider problem (1) with $L = 64$ and cubic nonlinearity. The initial ground state profile $u_{h,0}(x)$, $x \in [0,64]$, shown in Fig. 1, has been obtained by solving (16) with $J = 2400$; that is, $u_{h,0}(x)$ is a symmetric Hermite piecewise cubic polynomial in a uniform partition of 2400 subintervals of $[0,64]$. The parameter λ is initially estimated by the output value of the corresponding Lagrange multiplier in the resolution of (16), and it is approximately -3.5513497322095. This first estimate will be improved later by using other techniques.

With this initial profile and the spatial discretization implemented as explained in Section 3.1, we simulate the evolution of the corresponding ground state by using three time integrators: the SDIRK method (17), denoted by SD, its modified version with a projection on the particle number manifold SDNP and the method (17) with a projection to preserve the Ham-

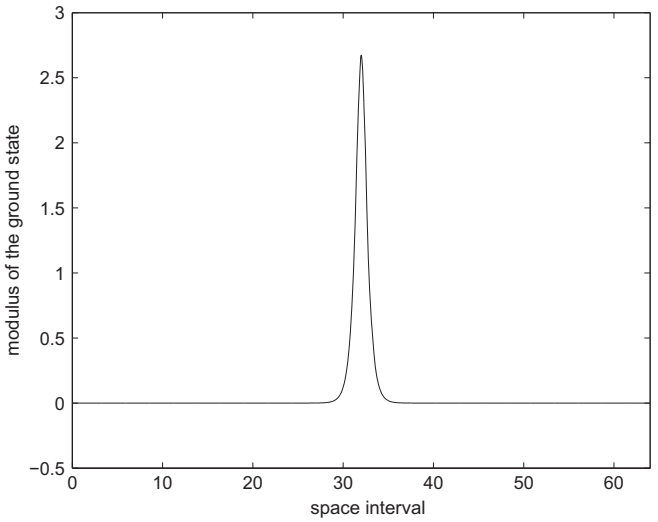

Fig. 1. Ground state in [0,64] with $J = 2400$ subintervals.

iltonian or SDHP method. In this case, it has not been possible to use the modified method with two projections, due to the singular character of the Jacobian matrix in the iterative process for (19). The reason is in formula (6), which establishes a dependence between the variational derivatives of the invariants at the ground state. This dependence also happens in the corresponding discretization and with the numerical ground state profile, showing the accuracy in the resolution of (16).

In Figs. 2 and 3, we have computed, respectively, the real and imaginary part of the numerical solution given by SDNP, from $t = 0$ to $t = 1000$, each fifty units of time. A modulated profile is observed.

The next numerical results are focused on the behaviour of the methods with respect to the invariants (2), (3) and the influence of the conservation properties on the simulation of the ground state parameters.

As far as the first question is concerned, Fig. 4 shows, in logarithmic scale, the time evolution of the relative error in the discrete approximations to N and H for the three methods above mentioned. In all cases, the time step is $\Delta t = 2.0d - 2$. Notice that relative errors generated by SD are bigger and show a temporal evolution. This growth with time disappears in the case of the other two methods. In the case of the two other schemes, Fig. 4 displays, for each of these two methods, the evolution of the error of the approximation to the quantity which is not preserved by the corresponding numerical method. That is, we measure errors in N for SDHP and errors in H for SDNP. We remark that the errors in the other quantity, due to the construction of the methods, are similar to precision used in the computation and they are not displayed.

It is of interest to notice that the two methods behave very well with respect to both quantities, even though they only preserve (at least in theory) one of them. This can also be explained by formula (6) and emphasizes again the good approximation provided by the initial profile (since an erroneous computation would affect the satisfaction of condition (16)).

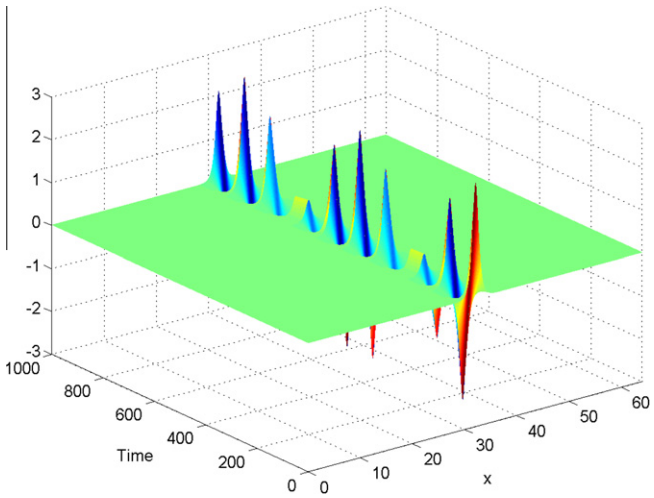

Fig. 2. Ground state simulation. Real part of the numerical solution given by SDNP. The time step is $\Delta t = 1.0d - 2$. The wave is plotted each 50 units of time, from $t = 0$ to $t = 1000$.

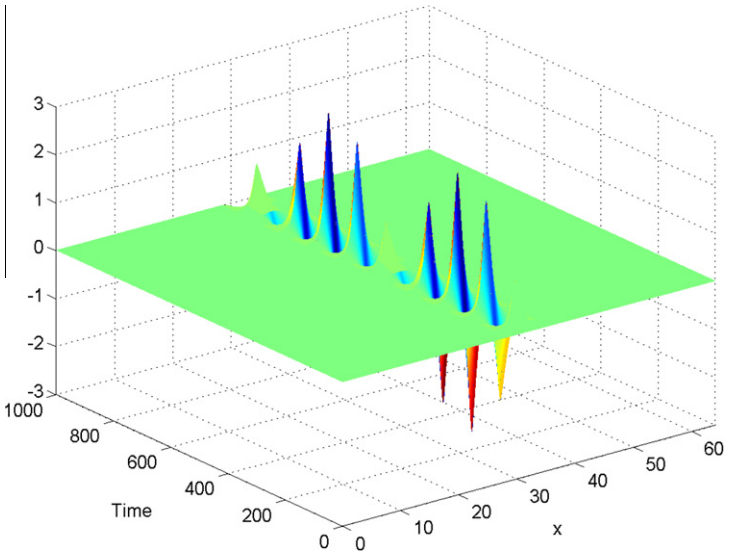

Fig. 3. Ground state simulation. Imaginary part of the numerical solution given by SDNP. The time step is $\Delta t = 1.0d-2$. The wave is plotted each 50 units of time, from $t = 0$ to $t = 1000$.

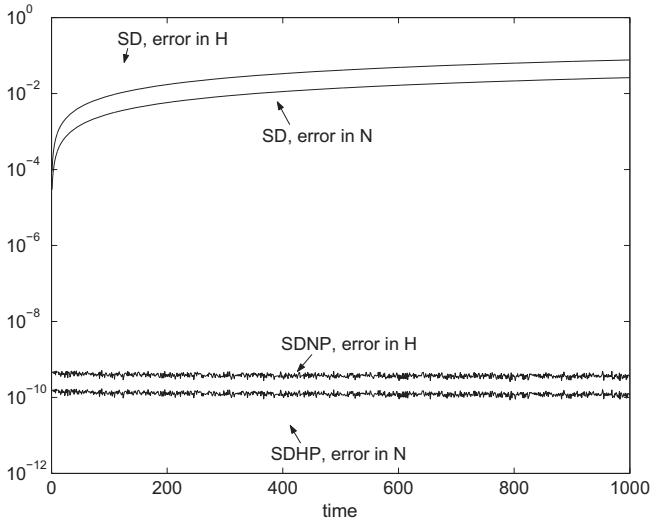

Fig. 4. Ground state simulation. Time evolution in logarithmic scale of the error in the invariants H and N for the three methods. The time step is $\Delta t = 1.0d-2$.

One of the consequences of the behaviour shown in Fig. 4 concerns the simulation of the angular velocity of the ground state, governed by λ. We carry out the computation of this parameter in two different ways. First, suppose that $\Phi_{j,n}$ denotes a numerical approximation to the solution at (x_j, t_n), $\Phi(x_j)e^{-i\lambda t_n}$; then, at this value of time, λ can be estimated as

$$\lambda \approx \frac{\arg\left(\frac{\Phi_{j,n-1}}{\Phi_{j,n}}\right)}{\Delta t} \tag{20}$$

The accuracy of the approximation depends in practice on x_j. We have obtained that, in our computations, the optimal choice is $x_j = 32$, where the maximum value of the discretized initial contour is achieved. Formula (20) is very cheap, in computational terms, and it can be easily implemented, but it requires a computation of the point where the approximation to the modulus of the ground state reaches a maximum value.

An alternative algorithm to the approximation of the angular velocity λ is as follows. Let Φ_h be the numerical solution which approximates a ground state. From (6) we have

$$\delta H(\Phi_h) + \lambda \delta N(\Phi_h) \approx 0.$$

Taking the inner product with Φ_h,

$$\langle \delta H(\Phi_h) + \lambda \delta N(\Phi_h), \Phi_h \rangle \approx 0. \tag{21}$$

By using the definitions of N and H, condition (21) means that

$$\int_0^L \left((\partial_{xx}\Phi_h)\overline{\Phi}_h + f\left(|\Phi_h|^2\right)|\Phi_h|^2 + \lambda |\Phi_h|^2 \right) dx \approx 0.$$

For the cubic case, $f(x) = x$. The previous integral turns into

$$\int_0^L \left(-|\partial_x \Phi_h|^2 + |\Phi_h|^4 + \lambda |\Phi_h|^2 \right) dx \approx 0,$$

that is

$$-2H(\Phi_h) + \frac{1}{2}\int_0^L |\Phi_h|^4 dx + 2\lambda N(\Phi_h) \approx 0,$$

which finally leads to

$$\lambda \approx \frac{1}{N(\Phi_h)} \left(H(\Phi_h) - \frac{1}{4}\int_0^L |\Phi_h|^4 dx \right). \tag{22}$$

Thus, formula (22) can also be used to estimate the value of λ. In the following experiments, and according to the suitability of the corresponding simulation, the alternatives (20) or (22) (or both) have been implemented, in order to study the influence of the time integrators on the simulation of λ. In this sense, both techniques lead to similar qualitative conclusions, as we will see below, but in some cases one of them is better than the other one. On the other hand, the approximation to the parameter λ may depend on the time t and the time step Δt. In the following experiments we will also analyze the contribution of these variables.

With the same initial data as above and the estimate (20), the time behaviour of the numerical parameter for the three methods is displayed in Fig. 5. This shows that the approximation to λ given by SD grows with time (in an, apparently, linear form) while the 'conservative' methods SDNP and SDHP simulate λ without any time evolution. In addition, they give a very similar approximation.

The constant in time behaviour of the simulation of λ given by SDNP and SDHP enables us to use them to estimate the angular velocity. It is also observed that this constant in time behaviour is independent of the step size. This can be seen in Fig. 6, which shows the evolution with time of the approximation to λ given by SDNP for $\Delta t = 4.0d - 2$, $2.0d - 2$ and by using both alternatives (20) and (22). It looks that both estimates of λ converge to a well defined value. Moreover, the values obtained with (22) seem to be better, although with bigger oscillations.

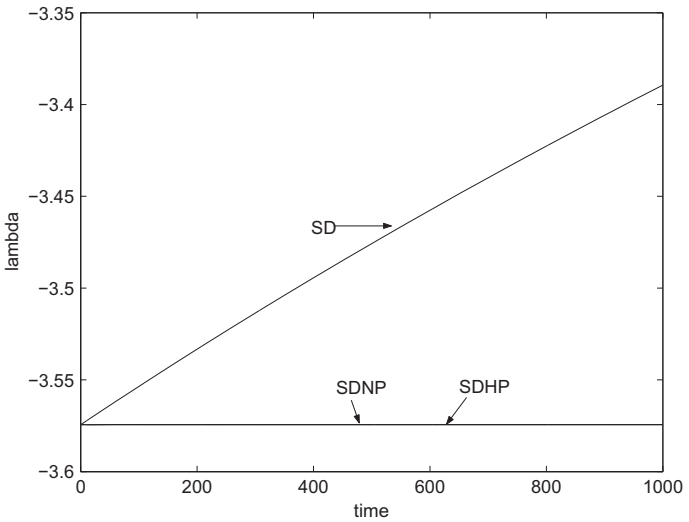

Fig. 5. Ground state simulation. Evolution of λ as function of time for the three methods. $\Delta t = 2.0d - 2$ and formula (20) are used.

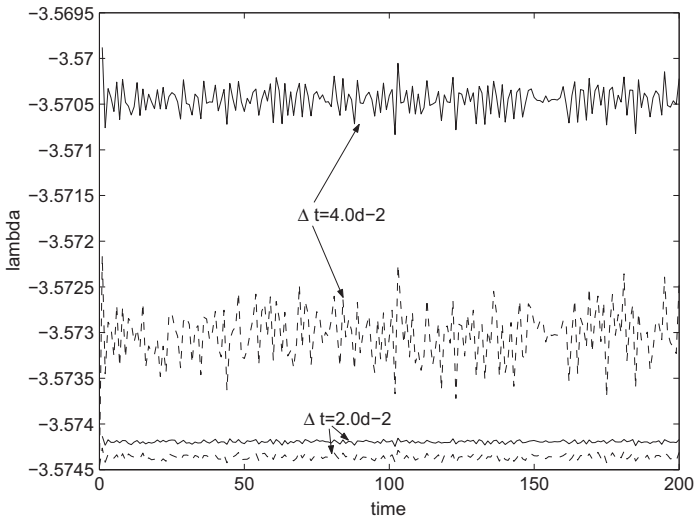

Fig. 6. Values of λ as function of time with $\Delta t = 4.0d-2, 2.0d-2$ for the method SDNP. Formula (20) with continuous line, and formula (22) with dashed line.

Once we have obtained a constant in time simulation of λ by using the conservative methods, a second point that affects the estimates of this parameter is the dependence on the time step size Δt, as Fig. 6 suggests. This will be discussed in the following experiments.

We first mention Tables 1 and 2. Second column of Table 1 shows, with the method SDNP and for the values of Δt considered in the first column, the corresponding estimates of the value of λ. In each case, this estimate has been obtained in the following way: the method SDNP has been run up to a final time $T = 200$ and every unit of time, an approximation to λ by using formula (20) has been computed. Then, the corresponding estimate which appears in Table 1 is the mean value of these approximations. The use of the mean value is justified by the fact that, by retaining the same accuracy, it achieves to rule out the oscillations (see Fig. 6). On the other hand, the third column is obtained from the second one by using Aitken extrapolation [8]. This is suggested in [27]. Finally, Table 2 shows similar contents, with the difference that (22) is used to compute the approximations to λ in the simulation, instead of (20).

Fig. 6 suggests some convergence of the approximations to a certain value of λ as Δt goes to zero. By considering the last extrapolated values in Tables 1 and 2 as references, Fig. 7 displays, in log–log scale, the errors as a function of Δt given by the values of the second column of the corresponding table. Stars correspond to Table 1 and circles correspond to Table 2. We observe that, in both cases, the slope of the lines suggests an $O(\Delta t^4)$ behaviour for the errors in the estimates, one more than the order $r = 3$ of the method.

According to the theory explained in [28] (see also [26]), in this case the numerical experiments suggest the following behaviour of the parameters θ and λ of (8) through the numerical integration. The numerical solution would contain a ground state profile $\Psi(x,t,\theta_n,\lambda_n)$ with parameters λ_n, θ_n which are perturbations of λ, θ, respectively, of the form

Table 1
Estimates of λ obtained with (20): mean values (first column) and extrapolation (second column).

Δt	Estimate	Extrapolation
$4.0d-2$	−3.57044930409735	
$2.0d-2$	−3.57419489201628	
$1.0d-2$	−3.57444597515882	−3.57446401569632
$5.0d-3$	−3.57446183068545	−3.57446289942784
$2.5d-3$	−3.57446281146187	−3.57446287613001

Table 2
Estimates of λ obtained with (22): mean values (first column) and extrapolation (second column).

Δt	Estimate	Extrapolation
$4.0d-2$	−3.57301675631360	
$2.0d-2$	−3.57436149583451	
$1.0d-2$	−3.57445626013480	−3.57446344449531
$5.0d-3$	−3.57446246365797	−3.57446289820361
$2.5d-3$	−3.57446286027564	−3.57446288736504

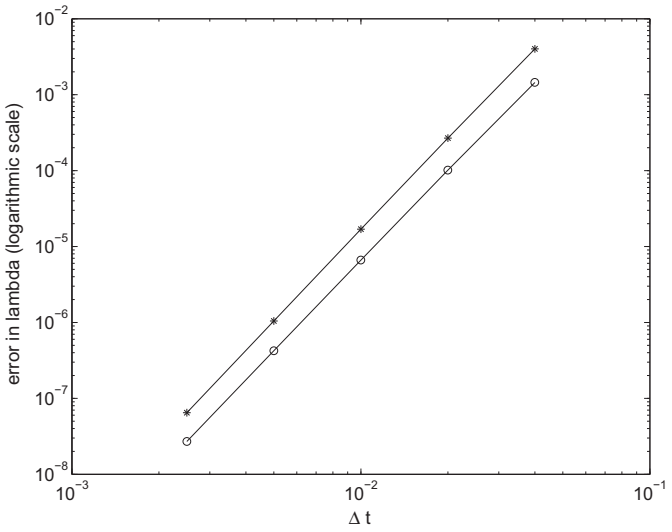

Fig. 7. Errors in λ versus $\Delta t = 4d-2$, $2d-2$, $1d-2$, $5d-3$, $2.5d-3$ with algorithms (20), stars, and algorithm (22), circles. Method SDNP.

$$\begin{aligned}\theta_n &= \theta + (\Delta t^r)\left(\alpha_1 + \beta_1 t_n + \beta_2 \frac{t_n^2}{2}\right) + O(\Delta t^{r+1}),\\ \lambda_n &= \lambda + (\Delta t^r)(\alpha_2 + \beta_2 t_n) + O(\Delta t^{r+1}),\end{aligned} \tag{23}$$

for some constants α_i, β_i, $i = 1, 2$, that depend on the integrator used and with r the order of the method ($r = 3$, in our case). This means that θ_n is a quadratic in time perturbation of the original phase, while λ_n differs from λ in linear in time terms. This would explain the behaviour of the method SD shown in Fig. 5 as follows. If we assume that the numerical solution is approximately a ground state profile of the form (8)

$$\Phi_{j,n} \approx \phi_j e^{-i\lambda_n t_n - i\theta_n} \tag{24}$$

with θ_n, λ_n given by (23), then, after some calculations, the estimate (20) is of the form

$$\frac{1}{\Delta t}\arg\left(\frac{\Phi_{j,n-1}}{\Phi_{j,n}}\right) = \lambda + (\alpha_2 + \beta_1)\Delta t^r + \Delta t^r \frac{3\beta_2}{2}(t_n + t_{n-1}) + O(\Delta t^{r+1}). \tag{25}$$

This gives the linear in time behaviour observed in Fig. 5 for the method SD.

The constant β_2 would vanish when the method is conservative [28]. In that case, the perturbation in θ would contain a first $O(\Delta t^r)$ term, which only grows linearly in time, while the perturbation in λ would include an $O(\Delta t^r)$ term, which is constant in time. That is, (23) would be of the form

$$\begin{aligned}\theta_n &= \theta + (\Delta t^r)(\alpha_1 + \beta_1 t_n) + O(\Delta t^{r+1}),\\ \lambda_n &= \lambda + (\Delta t^r)\alpha_2 + O(\Delta t^{r+1}).\end{aligned} \tag{26}$$

Now, (25) with $\beta_2 = 0$ explains the constant in time behaviour shown in Fig. 5 for the other two methods and the information suggested in Table 3 for the SDNP method. In both cases, the $O(\Delta t^{r+1})$ terms would also depend on time, see [26,27] and references therein.

The inclusion of the ansatz (26) in the computation of λ can also explain the behaviour shown in Fig. 7. We will take, for simplicity, formula (20) (the explanation for the other formula would be similar, although with a little more effort in the calculations). If (24) is assumed again, then, using (26), the estimate (25) takes the form

$$\frac{1}{\Delta t}\arg\left(\frac{\Phi_{j,n-1}}{\Phi_{j,n}}\right) = \lambda + (\alpha_2 + \beta_1)\Delta t^r + O(\Delta t^{r+1}). \tag{27}$$

Now, the use of the mean value and the Aitken method in the computations does not change the behaviour given by (27). Then, the comparison between these mean values and the estimate given by the last extrapolation forces the cancellation of the first two terms in (27) and shows the $O(\Delta t^{r+1})$ behaviour observed in Fig. 7 for the case of the method considered (with $r = 3$). Thus, the numerical solution provided by a conservative method would be more suitable, in the sense that it remains, for long times, closer to the 'orbit' of the solution.

An additional experiment illustrates these arguments. We have measured the differences, in maximum norm, between this numerical approximation and the ground state form $\Psi(x,t) = \Phi(x)e^{-i\lambda t}$, with the profile Φ obtained by solving (16) as

Table 3
Differences, in maximum norm, between the numerical solution and the ground state form with profile and velocity computed as in Section 4.1. SDNP with $\Delta t = 1.0d-2$.

Time	Real part	Imaginary part	Modulus
0	0	0	0
50	$3.0496d-6$	$3.1140d-6$	$4.2612d-6$
100	$1.6413d-3$	$1.9690d-3$	$6.6386d-6$
150	$2.1613d-6$	$2.4680d-6$	$5.5271d-6$
200	$5.0505d-3$	$9.0602d-4$	$8.3183d-6$
250	$3.0024d-6$	$1.0976d-3$	$5.6365d-6$
300	$6.6766d-3$	$2.7484d-6$	$6.0595d-6$
350	$2.4075d-6$	$6.8612d-3$	$7.2930d-6$
400	$3.5425d-3$	$2.2341d-6$	$6.8186d-6$
450	$2.1937d-6$	$1.1544d-2$	$3.7512d-6$
500	$3.6682d-6$	$3.1516d-6$	$4.0497d-6$
550	$9.0218d-3$	$1.0846d-2$	$8.0120d-6$
600	$2.8869d-6$	$2.7226d-6$	$4.1121d-6$
650	$1.6407d-2$	$2.9743d-3$	$6.8096d-6$
700	$2.5920d-6$	$3.0319d-3$	$3.7632d-6$
750	$1.6715d-2$	$2.5858d-6$	$6.2369d-6$
800	$2.6106d-6$	$1.5646d-2$	$6.3198d-6$
850	$7.5855d-3$	$2.9942d-6$	$1.0886d-5$
900	$2.4161d-6$	$2.3087d-2$	$4.9100d-6$
950	$3.1456d-6$	$3.7703d-6$	$5.2884d-6$
1000	$1.6355d-2$	$1.9762d-2$	$3.4916d-6$

previously explained, and the parameter λ computed with (20) at $t = 1$. The measures have been made each fifty units of time and up to $t = 1000$. They are displayed in Table 3. First and second columns show, respectively, the differences in the real and imaginary parts, while the third column corresponds to the comparisons between the modulus. The first two columns suggest and oscillatory linear growth. The combination of these results with those of the third column shows that this growth comes from differences localized in the phase.

4.2. Simulation of ground states with perturbations

The previous numerical experiments show that the simulation of ground states is more suitable when some properties of conservation of invariants of the problem are included into the features of the time integration. Furthermore, the advantages of the conservative methods are more relevant as the simulation is longer. This may lead to consider other situations where a longer time of integration is necessary. In this section, we study if the conservation properties of the time discretization contribute similar benefits in long time experiments involving ground state perturbations.

To this end, with the spatial discretization described in Section 3, we have used three different time integrators. First, the nonconservative method SD has been ruled out since, as we have seen before, it did not provide good results in ground state simulations any more. On the other hand, apart from the methods SDNP and SDHP, a third one has been designed, following the projection technique described above, in order to preserve the two quantities N and H. It will be denoted by SD2P. Notice that, since in the following experiments the initial condition will no longer be a ground state, then condition (6) does not hold; thus the variational derivatives of the quantities at the initial condition are not proportional and the two projections can be implemented.

In most of the numerical experiments to be shown in this section, initial profiles of ground states, generated by the technique described in Section 3, are subjected to small perturbations of different types. In these cases, the perturbed initial profile evolves to a more or less stable structure along with a sea of turbulence of different intensity. The structure seems to be a ground state, close to that of the unperturbed initial profile would generate. In this sense, the experiments confirm previous results in the literature [25,56]. For this group of experiments, we will establish some comparisons between the three methods, to select the most competitive one for the corresponding simulation.

A typical experiment consists of studying the evolution of initial ground state profiles which are perturbed in their parameters. Recall that the main parameter in the construction of the ground states is the angular velocity λ. An indirect way to study the effects of its perturbations is to observe the evolution of ground state profiles which are initially perturbed in the amplitude. As an illustration of this, in our case we have numerically integrated (1) for the cubic case with initial data given by a multiplicative perturbation of a ground state of the form $(1+10^{-3})\Phi_h(x)$, where $\Phi_h(x)$, $x \in [0,64]$, is a solution of (14) and is generated by the procedure described in Section 3.2. For this experiment, we will study the behaviour of the methods with respect to the invariants of the problem and to the parameters of the perturbed ground state.

4.2.1. Evolution of small perturbations of ground states

According to the ideas explained in the previous subsection, we focus on the simulation of the profile and the angular velocity of the emerging ground state. As far as the profile is concerned, the evolution of the perturbed initial data, with

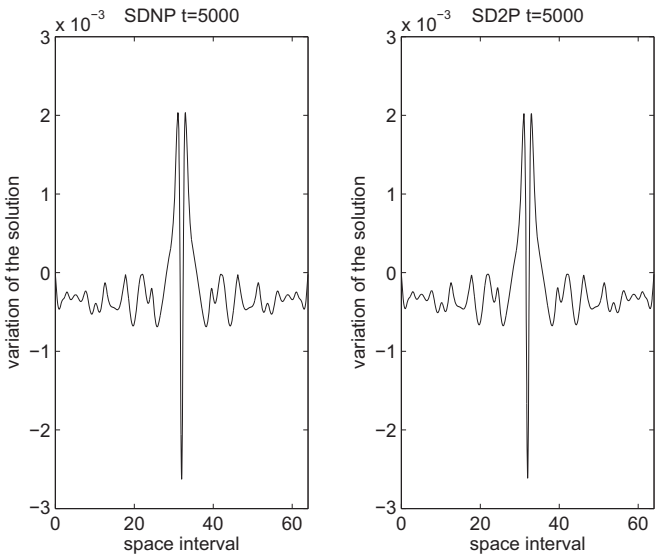

Fig. 8. Error between the modulus of the numerical solution at $t = 5000$ and the modulus of the initial profile. Left: SDNP and right: SD2P. The time step is $\Delta t = 1.0d - 2$.

any of the three methods, confirms the typical behaviour, above mentioned. By $t = 5000$, it is already clearly observed a ground state structure into the numerical solution. In Fig. 8 we display, for the methods SDNP and SD2P, the difference between the modulus of the corresponding numerical solution at $t = 5000$ and the modulus of the perturbed initial profile, for $\Delta t = 1.0d - 02$ (the method SDHP behaves like SDNP and this is not shown here). Note that the errors obtained are of the size of $1.0d - 03$. Then, we may consider the modulus of the corresponding numerical solution as the 'exact' profile and compare with the corresponding approximation for longer times. The comparison reveals some differences between the methods SDNP, SDHP and the method SD2P. Fig. 9 shows the difference between the modulus of the numerical solution, given by the SDNP method (at the top of the figure) and the SD2P method (at the bottom), at $t = 40{,}000$ and $t = 50{,}000$, and the corresponding modulus at $t = 5000$, with $J = 2400$ and $\Delta t = 1.0d - 2$ (the method SDHP displays similar results to those of SDNP method). We observe that the differences between the modulus are bigger for the case of the method SDNP. Fig. 9 also shows an increase with time in the two figures at the top which does not appear in the figures corresponding to the method SD2P.

The study of the preservation of the invariant quantities through the numerical integration for this initial condition makes evident some other differences between the methods. Fig. 10 shows the time evolution of the error in the Hamiltonian (the scale is logarithmic) for SDNP and SD2P with $J = 2400$ and $\Delta t = 1.0d - 2$. As expected, the method SD2P ensures a constant evolution of an almost imperceptible error. What is relevant here is the behaviour of SDNP, whose errors grow with time. Then we observe that, for these perturbations of the parameters of ground states, it seems to be necessary to ensure the numerical preservation of the two invariants of the continuous problem. This should be compared with the case of the simulation of an exact ground state, see Fig. 4. In that case, thanks to the condition (6), the preservation of one of the quantities guarantees the virtual conservation of the other one. This does not happen in this case. We have also compared, for the same initial condition, the errors in the quantity N for SDHP with a similar behaviour, since in this case errors in N grow with time.

This different behaviour also affects the estimates of the parameter λ of the new ground state profile. Fig. 11 shows the evolution of this parameter, computed with (20) and given by SDNP and SD2P. Observe that formula (22) is not suitable here, since the initial data is not an exact ground state. Although in both cases the estimate of λ is affected by noise, a different behaviour is clearly observed. In the case of SDNP, the oscillations are growing in amplitude as time evolves, unlike the evolution provided by SD2P. The information is summarized in Table 4, where we show the mean values and the maximum value of the oscillations for the estimates of λ computed with SDNP and SD2P in the first and second half time interval of computation. Notice that the values of λ change more quickly with the SDNP method than with SD2P.

4.2.2. Evolution with small nonlinear structures

The previous numerical experiments show that, in order to study small perturbations of the parameters of ground states, it seems advisable to consider two invariants preserving time integrators. We now study if this recommendation can also be given with other types of perturbations.

The general conclusion is that in other cases, the differences between the methods (and, consequently, the advantages of the numerical preservation of the two invariants) are not so clear. We have made computations with different perturbations from initial ground states, including various types of noise, purely nonlinear 'soliton' and initial Gaussian structures. As an illustration of all of them, we first consider the results obtained with an initial condition consisting of a ground state plus the small regular perturbation with a local support centered in $x = 16$,

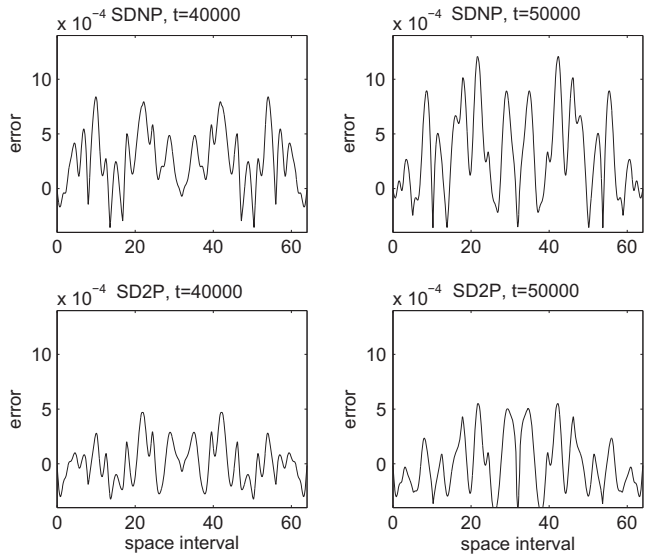

Fig. 9. Errors in the modulus of the numerical solution at $t = 40{,}000,\ 50{,}000$. Top: SDNP and bottom: SD2P.

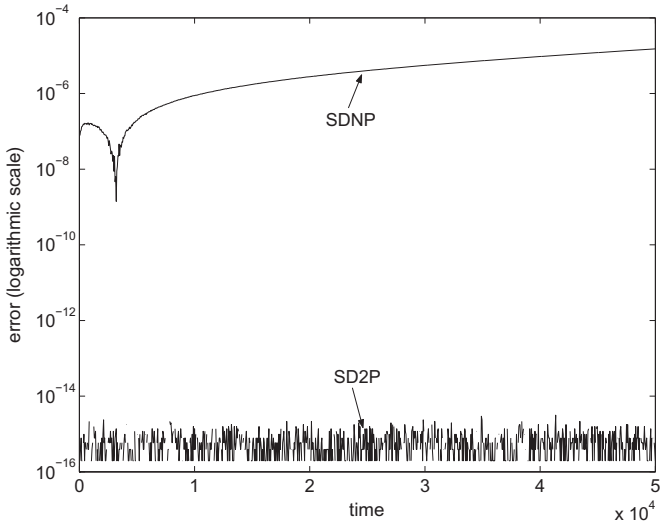

Fig. 10. Time evolution, in logarithmic scale, of the error in the invariant H for a multiplicative perturbation and methods SDNP, SD2P. The time step is $\Delta t = 1.0d-2$.

$$10^{-3}\exp\left(\frac{i}{8}(x-16)\right)\operatorname{sech}(2(x-16)),\quad x\in[0,64]. \tag{28}$$

The discretization in space has been carried out as above with $J = 2400$. For the time integration we have considered the three methods, SDNP, SDHP and SD2P. In each case the time step used has been $\Delta t = 1.0\mathrm{d}-2$. The evolution of this perturbed initial condition also follows, for the three methods, the usual behaviour previously described, with a coherent structure along with small noisy oscillations. Our goal here is again to compare the three numerical schemes in the analysis of the perturbed form.

The time evolution of the error in the Hamiltonian for SDNP and SD2P is displayed in Fig. 12. Notice that, although the error for SDNP continues to grow with time, this growth is less pronounced than that of the perturbation studied in the previous subsection (compare with Fig. 10 at the same time of computation). This better behaviour of the method SDNP has influence on the computation of the angular velocity parameter λ of the emergent ground state. This is shown in Table 5, where we notice that the difference between the two estimates for λ given by the two methods is approximately 10^{-6}, which is much smaller than the size of the perturbation.

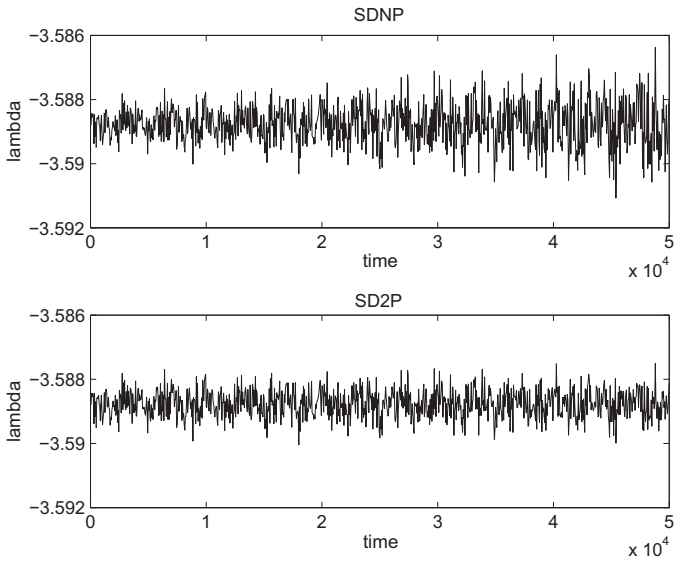

Fig. 11. Evolution of λ as a function of time for a multiplicative perturbation and methods SDNP, SD2P. The time step is $\Delta t = 1.0d - 2$.

Table 4
Mean values and maximum oscillations of λ for a multiplicative perturbation of a ground state and methods SDNP, SD2P.

Method	Time interval	Mean value	Max. oscillation
SDNP	[0,25,000]	−3.588754985013551	0.002832094837700
SDNP	[25,000,50,000]	−3.588750420406307	0.004699816136600
SD2P	[0,25,000]	−3.588758453331231	0.002354486698900
SD2P	[25,000,50,000]	−3.588760698083406	0.002482236264400

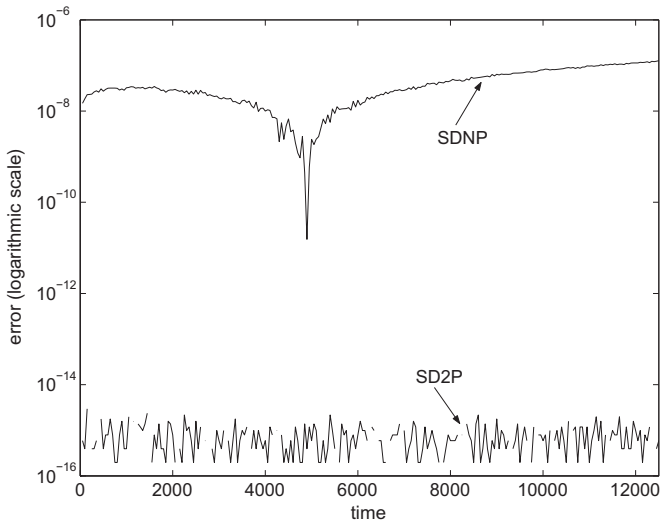

Fig. 12. Time evolution, in logarithmic scale, of the error in the invariant H for perturbation with (28) and methods SDNP, SD2P. The time step is $\Delta t = 1.0d - 2$.

Finally, it has to be pointed out that, for this experiment, SD2P is computationally slower. The reason may be in the form of the initial perturbation, which is of small size. This would imply that the perturbed solution does not separate very much from the orbit of a ground state, where SD2P fails due to the condition (6).

Table 5
Mean values and maximum oscillations of λ for a regular additive perturbation of a ground state, $t \in [0, 12{,}500]$.

Method	Mean	Max. oscillation
SD2P	−3.574445113133648	5.412890256000225e−004
SDNP	−3.574444631647461	5.776975272002716e−004

4.2.3. Evolution of an initial datum far from a ground state

We now study the problem with initial data far from a ground state. To this end, we consider

$$u_0(x) = \sqrt{2}\exp\left(\frac{iV}{2}x\right)\mathrm{sech}(x), \quad x \in [-30, 30], \tag{29}$$

where $V = 0.25$. In the case of the initial value problem, the evolution of this initial condition would generate a soliton, travelling with velocity V. However, for the problem on a finite interval and homogeneous Dirichlet boundary conditions, the solution behaves approximately as such a soliton while it is far of the boundary and, when the solution arrives at the boundary, it bounces into the interval.

The problem has been integrated with SDHP, SDNP, and SD2P. Fig. 13 shows, in logarithmic scale, the time evolution of the relative error in the invariant N for the three methods considered. Notice that the results obtained for the methods SDNP and SD2P are of the size of the precision used in the computation. Note also that, in the case of SDHP, the evolution grows with time. We have made the corresponding computations with respect to the error in the Hamiltonian, instead of the particle number, and we observe that, in that case, the growth with time is observed when SDNP is used. In both experiments, the best behaviour corresponds to SD2P. Therefore, the preservation of the two invariants seems recommendable for these initial data.

4.3. Evolution of two ground states as initial condition

A final question we have studied is the behaviour of the methods when the solution contains more than one ground state. To this end, the next experiment considers an initial condition consisting of a superposition of two ground states. For simplicity, we have chosen two structures with the same norm, but centered in $x = 16$ and $x = 32$, respectively. This arrangement allows to use (20) to compute the corresponding angular velocity parameters.

The form of the initial condition implies that the corresponding profile satisfies virtually two conditions of the form (6) and, consequently, the time integration cannot be carried out with the method SD2P. The other two methods, SDNP and SDHP, display a similar behaviour, which we explain by considering the results of the first one. The computations take $\Delta t = 1.0d - 2$ and $J = 2400$.

The behaviour of the method is essentially like that of the simulation of a ground state. Errors in the Hamiltonian are very small and almost constant during the simulation (see Fig. 14, which is run up to $t = 30{,}000$). The numerical solution shows a great stability near the initial condition. Computations involving the angular velocity parameters of the emergent ground

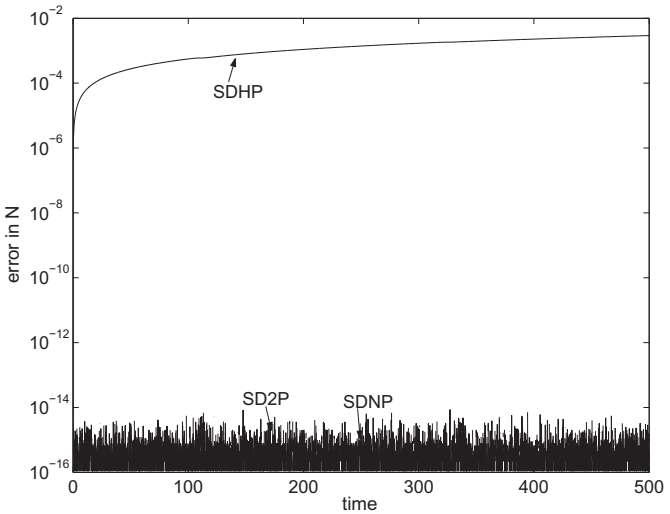

Fig. 13. Time evolution, in logarithmic scale, of the error in the invariant N for the initial condition (29) and methods SDNP, SDHP and SD2P.

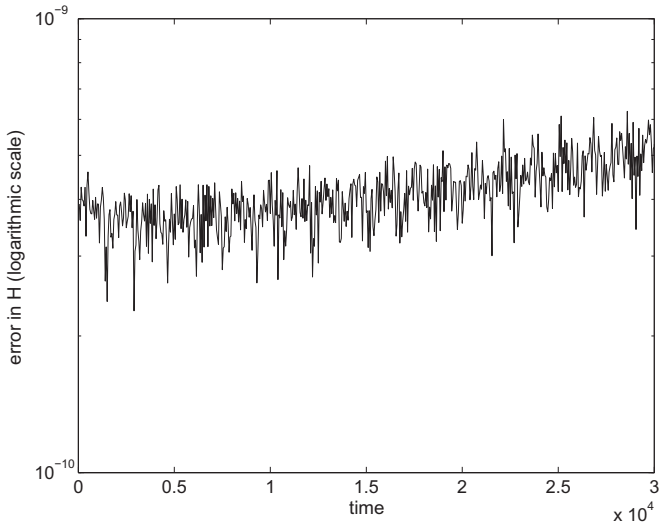

Fig. 14. Time evolution, in logarithmic scale, of the error in the invariant H for an initial condition with two ground states and the method SDNP. The time step is $\Delta t = 1.0d - 2$.

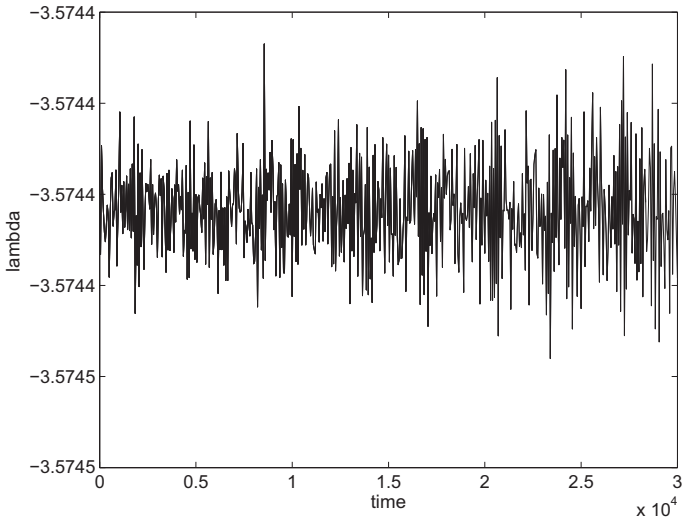

Fig. 15. Evolution of λ with time for the experiment with two ground states. Estimates with (20) for $x = 32$. SDNP method.

Table 6
Mean value and maximum oscillation of λ for the numerical solution with two ground states as initial condition. Method SDNP.

Time interval	Mean	Max. oscillation
[0,15,000]	−3.574445840625666	1.479130139969698e−005
[15,000,30,000]	−3.574445881556593	1.658681879979085e−005

states are displayed in Fig. 15 and Table 6. Both correspond to the ground state centered at $x = 32$ (the results at $x = 16$ are very similar). Table 6 shows the mean values and the maximum oscillation for the time intervals [0,15,000] and [15,000,30,000]. On the other hand, the time evolution of the estimate of λ with SDNP is observed in Fig. 15. Both show that the method, with only one projection, is still suitable for this kind of simulations, with more than one ground state, and the profiles well separated.

Acknowledgements

This research has been supported by MEC Project MTM2007-66343 cofinanced by FEDER funds; by MICINN Projects MTM2009-06507-E/MTM and MTM2010-19510/MTM; by Consolider Ingenio Mathematica Project MIGS-T4-0236 and by Junta de Castilla y León Projects JCYL VA040A07 and JCYL VA001A08.

References

[1] M.J. Ablowitz, J. Ladik, A nonlinear difference scheme and inverse scattering, Stud. Appl. Math. 55 (1976) 213–229.
[2] M.J. Ablowitz, Z.H. Musslimani, Spectral renormalization method for computing self-localized solutions to nonlinear systems, Opt. Lett. 30 (2005) 2140–2142.
[3] M.J. Ablowitz, H. Segur, On the evolution of packets of water waves, J. Fluid Mech. 92 (1979) 691–715.
[4] G.D. Akrivis, Finite difference discretization of the cubic Schrödinger equation, IMA J. Numer. Anal. 13 (1993) 115–124.
[5] G.D. Akrivis, V.A. Dougalis, O.A. Karakashian, On fully discrete Galerkin methods of second-order temporal accuracy for the nonlinear Schrödinger equation, Numer. Math. 59 (1991) 31–53.
[6] I. Alonso-Mallo, N. Reguera, A high order finite element discretization with local absorbing boundary conditions of the linear Schrödinger equation, J. Comput. Phys. 220 (2006) 409–421.
[7] X. Antoine, C. Besse, S. Descombes, Artificial boundary conditions for one dimensional cubic nonlinear Schrödinger equations, SIAM J. Numer. Anal. 43 (2006) 2272–2293.
[8] K.E. Atkinson, An Introduction to Numerical Analysis, Second ed., John Wiley & Sons, New York, 1989.
[9] W. Bao, Q. Du, Computing the ground state solution of Bose–Einstein condensates by a normalized gradient flow, SIAM J. Sci. Comput. 25 (5) (2004) 1674–1697.
[10] W. Bao, D. Jaksch, P.A. Markowich, Numerical solution of the Gross–Pitaevskii equation for Bose–Einstein condensation, J. Comput. Phys. 187 (2003) 318–342.
[11] W. Bao, S. Jin, P.A. Markowich, On time-splitting spectral approximations for the Schrödinger equation in the semiclassical regime, J. Comput. Phys. 175 (2002) 487–524.
[12] W. Bao, J. Shen, A fourth-order time-splitting Laguerre–Hermite pseudospectral method for Bose–Einstein condensates, SIAM J. Sci. Comput. 26 (2005) 2010–2028.
[13] W. Bao, W. Tang, Ground-state solution of Bose–Einstein Condensate by directly minimizing the energy functional, J. Comput. Phys. 187 (2003) 230–254.
[14] A. Boutet de Monvel, A.S. Fokas, D. Shepelsky, Analysis of the Global relation for the nonlinear Schrödinger equation on the half-line, Lett. Math. Phys. 65 (3) (2003) 199–212.
[15] J.P. Boyd, Why Newton's method is hard for travelling waves: small denominators, KAM theory, Arnold's linear Fourier problem, nonuniqueness, constraints and erratic failure, Math. Comput. Simul. 74 (2007) 72–81.
[16] D. Cai, D.W. McLaughlin, K. McLaughlin, The nonlinear Schrödinger equation as both a PDE and a dynamical system, Handb. Dyn. Syst. 2 (2002) 599–675.
[17] M. Caliari, G. Kirchner, M. Thalhammer, Convergence and energy conservation of the Strang time-splitting Hermite spectral method for nonlinear Schrödinger equations, preprint 2007.
[18] M. Caliari, A. Ostermann, S. Rainer, M. Thalhammer, A minimisation approach for computing the ground state of Gross–Pitaevskii systems, J. Comput. Phys. 228 (2009) 349–360.
[19] M.P. Calvo, J.M. Sanz-Serna, Numerical Hamiltonian Problems, Chapman & Hall, London, 1994.
[20] B. Cano, Conserved quantities of some Hamiltonian wave equations after full discretization, Numer. Math. 103 (2006) 197–223.
[21] E. Celledoni, D. Cohen, B. Owren, Symmetric exponential integrators with an application to the cubi Schrödinger equation, Found. Comput. Math. 8 (2008) 303–317.
[22] M.M. Cerimele, F. Pistella, S. Succi, Particle-inspired scheme for the Gross–Pitaevskii equation: An application to Bose–Einstein condensation, Comput. Phys. Commun. 129 (2000) 82–90.
[23] M. Delfour, M. Fortin, G. Payne, Finite-difference solution of a nonlinear Schrödinger equation, J. Comput. Phys. 44 (1981) 277–288.
[24] C.M. Dion, E. Cancès, Ground state of the time-independent Gross–Pitaevskii equation, Comput. Phys. Commun. 177 (10) (2007) 787–798.
[25] S. Dyachenko, V.E. Zakharov, A.N. Pushkarev, V.F. Shvets, V.V. Yankov, Soliton turbulence in nonintegrable wave systems, Sov. Phys. JETP 69 (1989) 1144–1147.
[26] A. Durán, Time behaviour of the error when simulating finite-band periodic waves. The case of the KdV equation, J. Comput. Phys. 227 (2008) 2130–2153.
[27] A. Durán, M.A. López-Marcos, Conservative numerical methods for solitary wave interactions, J. Phys. A: Math. Gen. 36 (2003) 7761–7770.
[28] A. Durán, J.M. Sanz-Serna, The numerical integration of relative equilibrium solutions, IMA J. Numer. Anal. 20 (2000) 235–261.
[29] M. Edwards, K. Burnett, Numerical solution of the nonlinear Schrödinger equation for small samples of trapped neutral atoms, Phys. Rev. A 51 (1995) 1382–1386.
[30] M. Edwards, R.J. Dodd, C.W. Clark, P.A. Ruprecht, K. Burnett, Properties of a Bose–Einstein condensate in an anisotropic harmonic potential, Phys. Rev. A 53 (4) (1996) 1950–1953.
[31] A. Eisner, B. Turkington, Nonequilibrium statistical behavior of nonlinear Schrödinger equations, Physica D 213 (2006) 85–97.
[32] G. Fibich, F. Merle, Self-focusing on bounded domains, Physica D 155 (2001) 132–158.
[33] A.S. Fokas, A.R. Its, The nonlinear Schrödinger equation on the interval, J. Phys. A: Math. Gen. 37 (2004) 6091–6114.
[34] D. Furihata, Finite-difference schemes for nonlinear wave equation that inherit energy conservation property, J. Comput. Appl. Math. 134 (2001) 37–57.
[35] M. Grillakis, J. Shatah, W. Strauss, Stability theory of solitary waves in the presence of symmetry, I, J. Funct. Anal. 74 (1987) 160–197.
[36] E. Hairer, C. Lubich, G. Wanner, Geometric numerical integration. Structure-preserving algorithms for ordinary differential equations, second ed., Springer-Verlag, Berlin, 2006.
[37] E. Hairer, S.P. Nørsett, G. Wanner, Solving Ordinary Differential Equations I. Nonstiff Problems, Springer Series in Computational Mathematics, second ed., vol. 8, Springer-Verlag, New York, Heidelberg, Berlin, 1993.
[38] A. Hasegawa, Self-organization processes in continuous media, Adv. Phys. 34 (1985) 1–42.
[39] A. Hasegawa, Y. Kodama, Solitons in Optical Communications, Oxford University Press, Oxford, 1995.
[40] A. Hasegawa, F. Tapper, Transmission of stationary nonlinear optical pulses in dispersive dielectric fibers. I. Anomalous dispersion, Appl. Phys. Lett. 23 (1973) 142–144.
[41] B.M. Herbst, J.L.I. Morris, A.R. Mitchell, Numerical experience with the nonlinear Schrödinger equation, J. Comput. Phys. 60 (1985) 282–305.
[42] http://www.nag.co.uk/numeric/fl/manual19/pdf/E04/e04ucffl19.pdf.
[43] R. Jordan, C. Josserand, Self-organization in nonlinear wave turbulence, Phys. Rev. E 61 (2000) 1527–1539.
[44] R. Jordan, C. Josserand, Statistical equilibrium states for the nonlinear Schrödinger equation, Math. Comput. Simul. 55 (2001) 433–447.
[45] R. Jordan, B. Turkington, C.L. Zirbe, A mean-field statistical theory for the nonlinear Schrödinger equation, Physica D 137 (2000) 353–378.

[46] A.L. Kassam, L.N. Trefethen, Fourth-order time-stepping for stiff PDEs, SIAM J. Sci. Comput. 26 (2005) 1214–1233.
[47] P.L. Kelley, Self-focusing of optical beams, Phys. Rev. Lett. 15 (1965) 1005–1008.
[48] T.I. Lakoba, J. Yang, A generalized Petviashvili method for scalar and vector Hamiltonian equations with arbitrary form of nonlinearity, J. Comput. Phys. 226 (2007) 1668–1692.
[49] T.I. Lakoba, J. Yang, A mode elimination technique to improve convergence of iteration methods for finding solitary waves, J. Comput. Phys. 226 (2007) 1693–1709.
[50] Y. Li, D. McLaughlin, Morse and Melnikov functions for NLS pdes, Commun. Math. Phys. 162 (1994) 175–214.
[51] Christian Lubich, On splitting methods for Schrödinger–Poisson and cubic nonlinear Schrödinger equations, Math. Comput. 77 (264) (2008) 2141–2153.
[52] J.E. Marsden, M. West, Discrete mechanics and variational integrators, Acta Numer. (2001) 357–514.
[53] T. Matsuo, D. Furihata, Dissipative or conservative finite-difference schemes for complex-valued nonlinear partial differential equations, J. Comput. Phys. 171 (2001) 425–447.
[54] D.E. Pelinovsky, Y.A. Stepanyants, Convergence of Petviashvili's iteration method for numerical approximation of stationary solutions of nonlinear wave equations, SIAM J. Numer. Anal. 42 (2004) 1110–1127.
[55] V.I. Petviashvili, Equation of an extraordinary soliton, Sov. J. Plasma Phys. 2 (1976) 257–258.
[56] Y. Pomeau, Asymptotic time behaviour of nonlinear classical field equations, Nonlinearity 5 (1992) 707–720.
[57] Y. Pomeau, Long time behavior of solutions of nonlinear classical field equations: the example of NLS defocusing, Physica D 61 (1992) 227–239.
[58] J.I. Ramos, Linearly implicit methods for the nonlinear Schrödinger equation in nonhomogeneous media, Appl. Math. Comput. 133 (2002) 1–28.
[59] P.A. Ruprecht, M.J. Holland, K. Burnett, M. Edwards, Time-dependent solution of the nonlinear SChrödinger equation for Bose-condensed trapped neutral atoms, Phys. Rev. A 51 (1995) 4704–4711.
[60] R. Salmon, L.D. Talley, Generalization of Arakawa's Jacobian, J. Comput. Phys. 83 (1989) 247–259.
[61] J.M. Sanz-Serna, Methods for the numerical solution of the nonlinear Schrödinger equation, Math. Comput. 43 (1984) 21–27.
[62] J.M. Sanz-Serna, J.G. Verwer, Conservative and nonconservative schemes for the solution of the nonlinear Schrödinger equation, IMA J. Numer. Anal. 11 (1991) 509–523.
[63] B.I. Schneider, D.L. Feder, Numerical approach to the ground and excited states of a Bose–Einstein condensed gas confined in a completely anisotropic trap, Phys. Rev. A 59 (3) (1999) 2232–2242.
[64] A. Scott, Nonlinear Science, Emergence and Dynamics of Coherent Structures, Oxford University Press, Oxford, 1999.
[65] W. Strauss, L. Vázquez, Numerical solution of a nonlinear Klein–Gordon equation, J. Comput. Phys. 28 (1978) 271–278.
[66] C. Sulem, P.L. Sulem, The nonlinear Schrödinger equation, self-focusing and wave collapse, Springer-Verlag, New York, 1999.
[67] V.E. Zakharov, Collapse of Langmuir waves, Sov. Phys. JETP 35 (1972) 908–922.
[68] T.R. Taha, A numerical scheme for the nonlinear Schrödinger equation, Comput. Math. Appl. 22 (1991) 77–84.
[69] Y.F. Tang, L. Vázquez, F. Zhang, V.M. Pérez-García, Symplectic methods for the nonlinear Schrödinger equation, Comput. Math. Appl. 32 (1996) 73–83.
[70] M. Thalhammer, M. Caliari, Ch. Neuhauser, High-order time-splitting Hermite and Fourier spectral methods, J. Comput. Phys. 228 (3) (2009) 822–832.
[71] J.A.C. Weideman, B.M. Herbst, Split-step methods for the solution of the nonlinear Schrödinger equation, SIAM J. Numer. Anal. 23 (1986) 485–507.
[72] M.I. Weinstein, Modulational stability of ground states of nonlinear Schrödinger equations, SIAM J. Math. Anal. 16 (1985) 473–491.
[73] V.E. Zakharov, S.V. Manakov, Complete integrability of the nonlinear Schrodinger equation, Teor. Mat. Fiz. 19 (1974) 332–343.
[74] V.E. Zakharov, A.B. Shabat, Exact theory of two-dimensional self-focusing and one-dimensional self-modulation of waves in nonlinear media, Sov. Phys. JETP 34 (1972) 62–69.
[75] F. Zhang, V.M. Pérez-García, L. Vázquez, Numerical simulation of nonlinear Schrödinger systems: a new conservative scheme, Appl. Math. Comput. 75 (1995) 165–177.
[76] Ch. Zheng, Nonreflecting boundary conditions for one-dimensional cubic nonlinear Schrödinger equations, J. Comput. Phys. 215 (2006) 552–565.